A three-dimensional cell-laden microfluidic chip for *in vitro* drug metabolism detection

2014 Biofabrication 6 025008

(http://iopscience.iop.org/1758-5090/6/2/025008)

IOP Publishing Biofabrication
Biofabrication 6 (2014) 025008 (13pp) doi:10.1088/1758-5082/6/2/025008

A three-dimensional cell-laden microfluidic chip for *in vitro* drug metabolism detection

Qudus Hamid[1], Chengyang Wang[1], Yu Zhao[2], Jessica Snyder[1] and Wei Sun[1,2,3]

[1] Department of Mechanical Engineering and Mechanics, Drexel University, Philadelphia, PA, USA
[2] Mechanical Engineering and Biomanufacturing Research Institute, Tsinghua University, Beijing, People's Republic of China
[3] Shenzhen Biomanufacturing Engineering Laboratory, Shenzhen, Guangdong, People's Republic of China

E-mail: sunwei@drexel.edu

Received 15 August 2013, revised 11 February 2014
Accepted for publication 12 February 2014
Published 3 April 2014

Abstract

Three-dimensional tissue platforms are rapidly becoming the method of choice for quantification of the heterogeneity of cell populations for many diagnostic and drug therapy applications. Microfluidic sensors and the integration of sensors with microfluidic systems are often described as miniature versions of their macro-scale counterparts. This technology presents unique advantages for handling costly and difficult-to-obtain samples and reagents as a typical system requires between 100 nL to 10 μL of working fluid. The fabrication of a fully functional cell-based biosensor utilizes both biological patterning and microfabrication techniques. A digital micro-mirror (photolithographic) system is initiated to construct the tissue platform while a cell printer is used to precisely embed the cells within the construct. Tissue construct developed with these technologies will provide an early diagnostic of a drug's potential use. A three-dimensional interconnected microfluidic environment has the potential to eliminate the limitations of the traditional mainstays of two-dimensional investigations. This paper illustrates an economical and an innovative approach of fabricating a three-dimensional cell-laden microfluidic chip for detecting drug metabolism.

Keywords: drug metabolism, microfluidic, tissue-on-a-chip, cell-laden chip

(Some figures may appear in colour only in the online journal)

1. Introduction

Microelectromechanical systems (MEMS) were popularized with the introduction of the integrated circuit (IC). Since then, MEMS technologies have been utilized in many fields with great success [1–5]. Micro-molding, etching, and deposition of features on or in materials are frequently referred to as microfabrication [6–10]. These techniques enable the creation of biologically inspired systems. Microfabricated constructs often possess a combination of structural and mechanical features that aid, but are not limited to, the development of micro-scale devices for pharmaceutical applications [11, 12]. The unique advantage of a microfluidic system is its ability to increase the surface area-to-volume ratio and the omnipresence of laminar fluid flow [13, 14]. Advancement of computation power has led to the ability to produce micro-features on a digital platform and decreases the fabrication time and cost of each device [15–17]. Presently, chemical and biological sensors are delicate, complex devices with a very limited range and scope that do not accurately predict the human response to environmental toxins. Furthermore, molecular sensors are capable of detecting only single pathogens or chemicals [18–23]. The limitations of biological sensors are primarily associated with two-dimensional culture on tissue culture plastic which has been a mainstay in conventional cell culture by dispersing complex tissues into single cells and ignoring higher-order processes [24]. Many tissue-based sensors are developed with microfabrication and layered biofabrication technologies. The cell signaling pathway components in these

sensors are highly discriminating and have a sensitive detection mechanism for identifying a wide range of pathogens and chemicals. More robust sensors based on three-dimensional tissue and/or organ fragments may then be used to rapidly detect biological or chemical threats under a variety of conditions and scenarios. Tools of biofabrication technologies may enable the development of increasingly sophisticated tissue analogues capable of processing complex environmental information and potentially serving as smart sensors in public health surveillance [25–28].

In the field of tissue engineering and regenerative medicine, three-dimensional cell printers are used to develop tissue scaffolds and building blocks for the generation and regeneration of functional tissue. The patterning of cells on surfaces is utilized for the development of biosensors, biomedical devices, and aids in the investigation of fundamental cell biology questions [29–33]. The search for drugs demands robust and fast methods to find, refine, and test probable drug candidates. Integrating the advances in the tissue engineering and microfabrication fields creates a potential to develop biosensors that will produce tissue arrays for pharmaceutical investigations. These sensors can potentially characterize pathogens, toxicants, odorants, and detect drugs within a given sample(s) [34–36]. Most biosensors developed within this integrated field are simplified or advanced devices that allow for faster and accurate characterization [37]. These sensors do not change the nature of molecular reaction, molecular diffusion, or heat transport governing laws. The need for a three-dimensional sensor for pharmaceutical investigations is overwhelming.

Investigations presented in this paper demonstrate the fabrication of an interconnected three-dimensional tissue array for pharmaceutical investigations. This platform was developed in part to function as a biosensor. This sensor can provide a micro three-dimensional environment for cells to attach, proliferate and differentiate. One unique advantage of this sensor is its laminar fluid flow within the pores of the chip [38]. The combination of a three-dimensional architecture and laminar fluid flow makes this sensor a prime candidate for drug characterizations [39]. A digital microfabrication device (photolithographic) is activated to fabricate the internal architecture of sensor. The enclosure of this biosensor is constructed with the use of micro-molding fabrication technique. All surfaces of the interconnected architecture are chemically enhanced with the use of a micro freeform dielectric barrier discharge (DBD) plasma treater. This surface enhancement provides the appropriate chemical and mechanical cues necessary for proper cell attachment and proliferation [40, 41]. The surface functionalization illustrated is cell specific and can be regulated for single or multiple cell [42] studies.

A combination of several tissue engineering and microfabrication techniques was utilized to develop the sensor presented in this paper, namely; (1) a digital micro-mirror device (DMD), (2) a freeform micro-plasma system, and (3) a multi-nozzle biological deposition system. (1) The DMD is a digital light processing unit that projects images of '.jpeg', '.bitmap', or '.gif' formats. The micro-mirrors have the option to switch between masks within a matter of microseconds, while offering high resolutions performance in spatial light modulation. With ultraviolet (UV) light, this component offers a flexible platform to design and develop proof of concepts, tissue models, biosensors, and micro-organs. (2) The DBD technique ignites the plasma which is then delivered through a micro-nozzle. DBDs are non-equilibrium plasmas operated under atmospheric pressure [43]. Due to a non-equilibrium nature, DBD plasmas can generate high energy electrons at cool background gas temperatures (heavy particles). This unique application of a selective high electron temperature, and low background temperature enables a rich plasma chemistry in many plasma chemical processes [44]. Once the micro-plasma is generated, it contacts the surface of biopolymer and changes the topography and chemistry of the plasma-exposed area. (3) The multi-nozzle biologics deposition system is capable of depositing heterogeneous materials, cell types, and biological factors in a controlled and reproducible manner [45–47]. Cell printing is considered to be an effective tool in the field of tissue engineering to assemble biologics. This printer executes micron-scale spatial control to generate cell-laden constructs.

2. Methods and materials

The sensors presented in this paper are fabricated from two materials. Polydimethylsiloxane (PDMS) (Dow Corning, Michigan, USA), is used as the base of the chip while SU-8 2100 (MicroChem Corp, Newton, MA, USA) is used to fabricate the internal micro-architecture of the chip. Details of the fabrication procedures are presented below. The biological investigation used MDA-MB-231 (human breast adenocarcinoma) cell line obtained from American type culture collection (ATCC) (Virginia, USA). This cell line is chosen to characterize the model's potential to develop a drug model. Unless listed otherwise, all cell culture supplements were obtained from ATCC. All biological investigation data are expressed as the mean $\pm$ standard deviation for sample size of 3 ($n = 3$).

2.1. System overview

2.1.1. Digital micro-mirroring. The main component of this system is the DMD, an optical semiconductor module that allows for the digital manipulation and projection of UV light. A computer system is integrated with this microfabrication system to operate the digital mirrors. The mirrors are mounted directly above the platform and are angled toward the UV light source. The UV source is adjustable in terms of intensity and exposure time. The light from the UV lamp travels and uniformly distributes on the micro-mirrors. During the projection phase, the digital mirrors would either be 'on' or 'off' depending on the pattern being projected. Mirrors that are turned 'on' would absorb the UV light and project it downward onto the substrate, while mirrors that are turned 'off' would reflect the UV light in the opposite direction [48]. Figures 1(*A*) and (*B*) features a flow chart of the digital micro-mirroring illustrating the connectivity and functionality of each

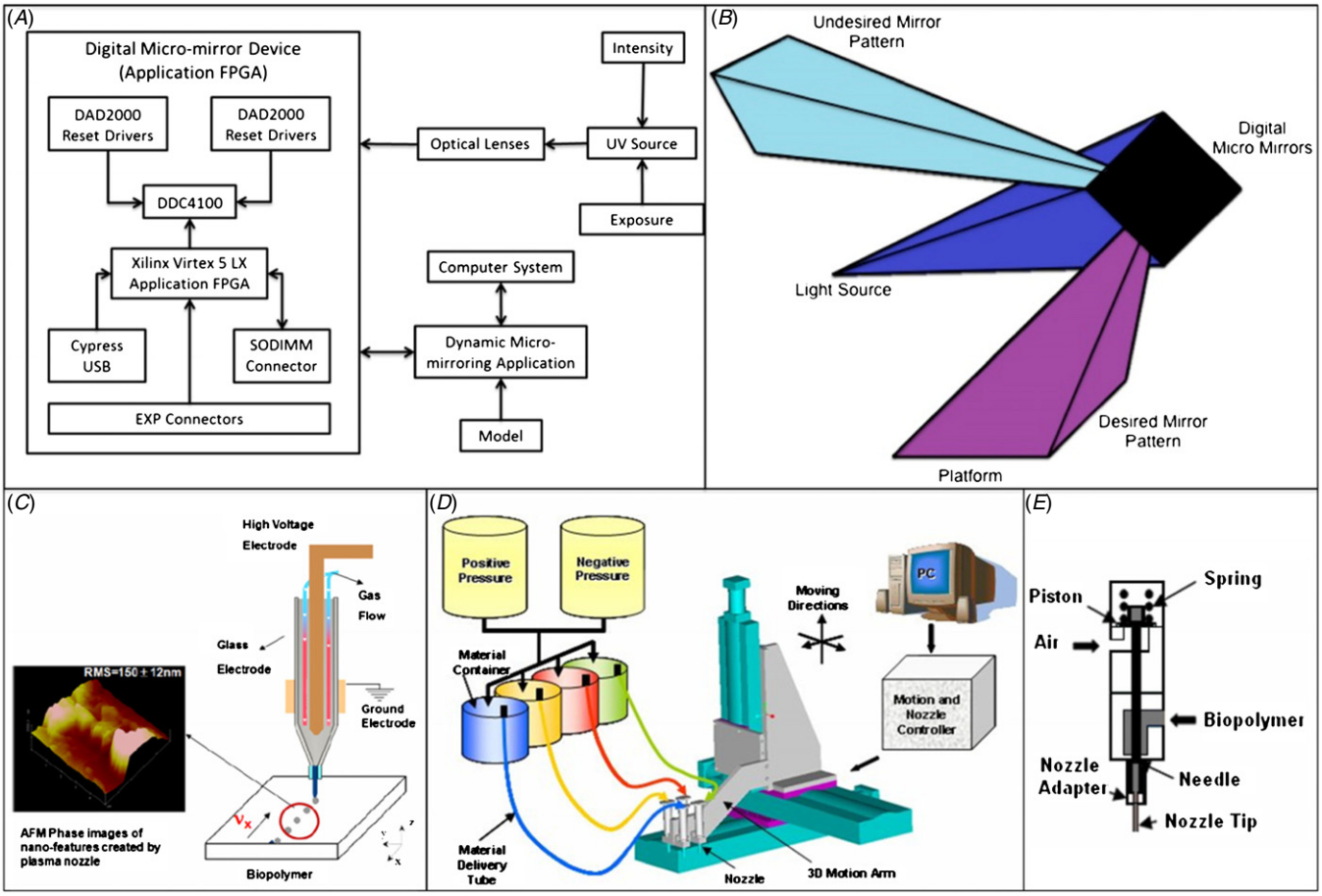

Figure 1. (*A*) A flow chart of the digital micro-mirroring illustrating the connectivity and functionality of each major component of the system. (*B*) A schematic of the digital mirror which shows the source light projected onto the mirrors and the direction in which the light is reflected. The 'desire' light projects pattern downward toward the platform and the unwanted light is projected away from the platform. (*C*) A schematic showing the cross-section of the micro-plasma nozzle treating the surface of a substrate. The major components of the nozzle are shown along with a photo of a treated sample is illustrated to demonstrate the effects of the micro-plasma nozzle. (*D*) A schematic of the freeform system which houses the micro-plasma nozzle and the biological deposition nozzle. (*E*) A cross-sectional schematic of the major components of the biological nozzle and the flow of the fluids through the nozzle.

major component of the system and a schematic of the digital mirror which shows the source light projected onto the mirrors and the direction in which the light is reflected. The 'desire' light projects pattern downward toward the platform and the unwanted light is projected away from the platform. The internal architecture of the chip is fabricated using this device. This system is utilized for the second phase of the fabrication process. This phase is responsible for the fabrication of the internal architecture of the chip.

2.1.2. Freeform micro-plasma. The DBD technique generates non-thermal plasma through a 30 μm micro-nozzle. The micro-plasma is generated by a pulsed power supply with a variable frequency. Connected to the power supply is the plasma electrode system with a high voltage electrode coaxially inserted in a dielectric tube of either borosilicate glass or quartz with a ground electrode wrapped about the outside of the tube. The process gas (or gas mixture) is purged through the annular gap between the coaxial electrode and the dielectric tube. When the high voltage electrode is powered, plasma is ignited between the electrodes and a micron-scale glow-like plasma will appear at the tip of the nozzle. The plasma generated at the tip of the nozzle is utilized for the third phase of the fabrication process. This phase uses the plasma to change the topography and chemistry of the plasma-exposed area. This phase of the fabrication process is a critical component in the development of the interconnected tissue array as it is responsible for the biological enhancement of the chip. Figure 1(*C*) shows a schematic of the cross-section of the micro-plasma nozzle treating the surface of a substrate. As seen in figure 1(*C*), nano features are created by the plasma nozzle. The nano features created by the plasma nozzle changes the topology of the substrate. Combined with the surface chemistry changes, this process would make a hydrophobic substrate more hydrophilic. In this case, the SU-8 is a hydrophobic substrate and the changes in the topology and surface chemistry allows for a hydrophilic substrate. This change allows for cells to attach onto the surface of the channels and actively proliferate. Without the nano features and the enhanced surface chemistry, cells will not attach onto the channels and the chip would fail.

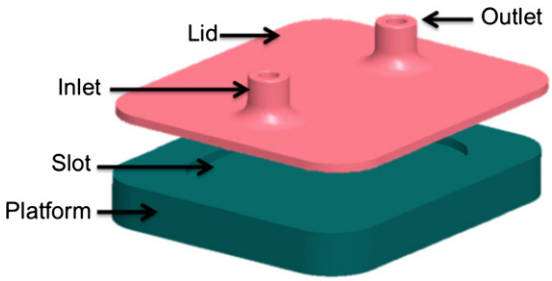

Figure 2. A model of the PDMS enclosure of the microfluidic chip.

2.1.3. Multi-nozzle biologics deposition. This system is inspired by rapid prototyping technology and is built on a CAD/CAM platform. The biologics printer operates with the cell-friendly conditions of room temperature and low pressure conditions. This system consists of three motion arms for three-dimensional spatial control and a material deposition which houses up to four biological materials at once. The deposition system utilizes micro-valve nozzle systems that can deposit numerous solutions with a wide range of material and biological properties. The computer controlled multi-nozzle biologics deposition system eliminates human errors and provides its users with precision control during fabrication procedures. This printer executes micron-scale spatial control to generate cell-laden constructs. The final phase of this fabrication process utilizes this system to precisely deposit cells into the micro-channel. With its unique ability of precision and control, this system enables the user to seed cells into the construct of any complex architecture. This allows for uniform cell seeding throughout the chip. Figure 1(*C*) shows a schematic of the freeform system which houses the micro-plasma nozzle and the biological deposition nozzle. The cross-sectional schematic of the major components of the biological nozzle and the flow of the fluids through the nozzle are featured in figure 1(*D*).

2.2. Fabrication protocol

Fabricated entirely from PDMS, the enclosure of the sensor is developed to house the internal features. The enclosure comprises of a platform (bottom) and a lid (top). The inlet and outlet ports are a nylon based luer-lock port (McMaster-Carr, Robbinsville, NJ, USA). PDMS is mixed at 1:15 ratio, de-gassed and cured in an aluminum mold at 130 °C for 10 min. The cured PDMS is cooled and removed from the aluminum mold. This process is repeated for the lid where the luer-lock ports are placed into position prior to being cured on the hot plate. Figure 2 illustrates a model of the PDMS enclosure.

SU-8 is a chemically amplified, epoxy-based negative photoresist typically used for producing ultra-thick resist layers during device manufacturing in the semiconductor industry. However, as a hydrophobic material, the use of SU-8 is limited due to the high degree of non-specific adsorptions of biomolecules, as well as limited cell attachment [49]. The structural integrity and photo-chemical properties of SU-8 makes this material an ideal candidate for the fabrication of micro-structures. The biological enhancement of SU-8 which allows for cell attachment, proliferation, and differentiation is presented below. The fabrication of the internal features starts by pouring and leveling SU-8 within the PDMS slot (bottom of the enclosure). The bottom enclosure with the SU-8 is soft-baked at 65 °C for 20 min, then at 90 °C for 220 min for stability. Immediately after soft-baking, it is cooled for 30 min then exposed at the recommended exposure time based on the amount of energy required for crosslinking (provided by the manufacturer). The exposure time with the use of the digital mirrors is 10.75 min, a total exposure of 557 mJ. The exposed sample is then hard baked at 65 °C for 15 min, then at 90 °C for 30 min for structural integrity. Prior to development with the SU-8 Developer (MicroChem Corp, Newton, MA, USA), samples are cooled for another 30 min. During the development process, all unwanted SU-8 will be washed away. The total development time per sample is 8–15 min. After development, samples are removed and rinse with deionized water to remove any excessive materials within the channels.

The second layer follows the same protocol for soft-baking, exposure, hard-baking, and development. The fabrication of the second layer begins with creating a PDMS enclosure; this enclosure is as thick as the first layer (500 μm). As listed above, enclosure for the second layer follows the same fabrication protocol as the fabrication of the bottom enclosure. After the enclosure is cooled, it is placed on a piece of glass (due to the curing ratio of the PDMS, the PDMS sticks to the glass without any leaks). SU-8 is then poured and leveled within the enclosure followed by soft-baking, exposure, hard-baking, and development with the same protocol as the first layer. Figure 3(*A*) shows a schematic of the fabrication and assembly of the cell-laden microfluidic chip.

Three chips are featured in this paper with varying porosity. The width of the channel directly affects the fluid flow; the wider the channel becomes the more turbulent the flow becomes. To maintain a laminar flow within the chip, the channels should be as small as applicable to the chip's functionality. Hence, the width of should not exceed 1 mm. If the channel's width exceeds 1 mm its environment can no long be considered a microfluidic environment. With the upper limit established, a lower limit will present an acceptable range to select three varying pore sizes. A cell's diameter ranges from 5 up to 50 μm. For cell to have a good cell–cell interaction there must be multiple cells together. This means the minimum channel width should allow for at least four cells to attach perpendicular (side by side) to the fluid flow. Hence, the minimum width should be 200 μm. With the acceptable range being 200–1000 μm; the three chips selected, features a low, mid, and upper range microchannels. Several fabricated 3D tissue scaffold features a pore size of 200–500 μm [50, 51]. The first two chips of pores 300 and 500 μm will investigate the difference of the upper and lower limits of the preferred 3D scaffold pores in a microfluidic chip. The final chip of 700 μm was selected to investigate the benefits of a larger microchannel chip. Together, these three chip sample will give a board idea of the cells' functionality in a three-dimensional laminar biological microfluidic chip. Figure 3(*B*)–(*D*) shows three schematics illustrating the micro-channel orientation of the first and second layers of the micro-fluidic chip along with a schematic of the two layers overlapping each other for the 300, 500, and 700 μm micro-fluidic chips.

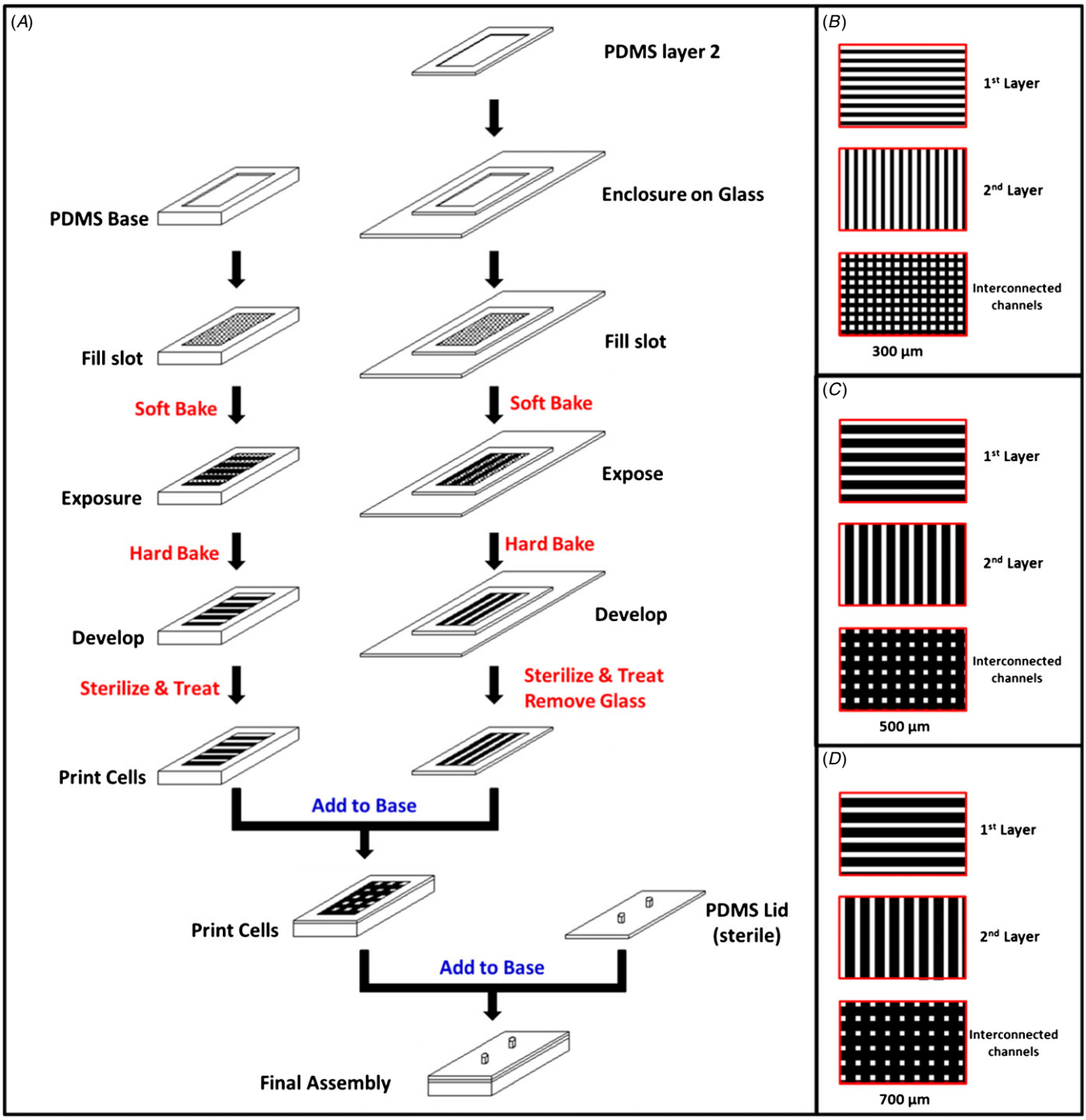

Figure 3. (*A*) A schematic of the fabrication and assembly of the cell-laden microfluidic chip. (*B*) A schematic illustrating the micro-channel orientation of the first and second layers of the chip along with a schematic of the two layers overlapping each other for the 300 μm chip, the black bars represents the channel walls and the white bars are the channels. (*C*) A schematic illustrating the micro-channel orientation of the first and second layers of the chip along with a schematic of the two layers overlapping each other for the 300 μm chip, the black bars represents the channel walls and the white bars are the channels. (*D*) A schematic illustrating the micro-channel orientation of the first and second layers of the chip along with a schematic of the two layers overlapping each other for the 300 μm chip, the black bars represents the channel walls and the white bars are the channels.

2.3. Sterilization, plasma treatment, and cell printing

Sterilization is a critical process whenever samples have to undergo biological characterization. There are several sterilization methods available; however, the appropriate method must be chosen in order to prevent any deformation or unwanted changes to the samples. Since the materials used to fabricate the biosensor are insensitive to high temperatures, the authors have found that a dry heat sterilization process of 150 °C will suffice.

Prior to cell deposition within the micro-channels, all samples are plasma treated with the in-house freeform micro-plasma. The gas composition used for treatment is 5% oxygen and 95% helium [40, 41]. The plasma nozzle

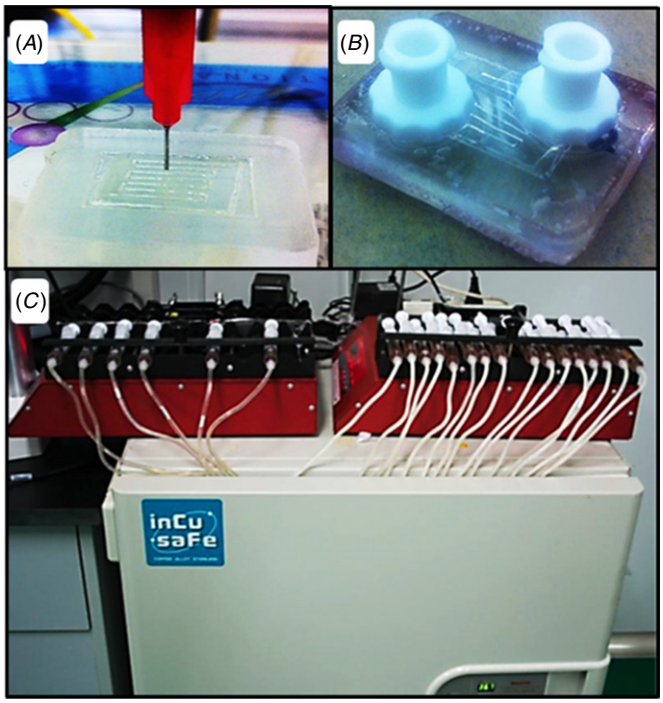

Figure 4. (*A*) A photo of the biologic deposition nozzle printing cells into the channels of the chip. (*B*) A photo of a fully fabricated chip, complete with enclosure, inlet and outlet ports (white), and internal features. (*C*) A photo of the incubation period of the chips where the syringe pump perfuse culture medium through the chips.

is programmed to first treat the PDMS (enclosure); plasma treating the PDMS will create a seal between the PDMS-to-PDMS contact. The second phase of plasma treatment is treating the SU-8 features for which the micro-nozzle allows precise treatment of the channels. Immediately after treatment, the multi-nozzle biologics deposition device prints cells within the channels. Figure 4(*A*) shows a photo of the biologic deposition nozzle printing cells into the channels of the chip. Once the cells are printed within the first layer of the chip, the second layer is placed on top of the first layer after being plasma treated (same protocol as the first layer). The plasma treatment changes the functionalization of the PDMS and SU-8 which creates a seal between the layers and provides an environment for cells to attach and proliferate. The chip is complete once the lid is placed on top of the second layer, after cells are deposited within the channels of the second layer. Figure 4(*B*) shows a photo of a fully fabricated chip, complete with enclosure, inlet and outlet ports (white), and internal features. Once the cell-laden chip was sealed, it was immediately placed in the incubator with a fluid line connected to the inlet and outlet of the chips for a total duration of 14 days where culture medium was perfused continuously through the chips with the use of a syringe pump at a flow rate of 30 μL h^{-1} During this time span, several biological characterizations are conducted at various time points. Figure 4(*C*) shows a photo of the incubation period of the chips where the syringe pump perfuse culture medium through the chips.

The working cell suspension that is loaded into the biological nozzle utilized the MDA MB 231 cell line. The confluent MDA MB 231 cells were harvested and counted from 75 cm^2 vented flasks using hemocytometer. Cells were then re-suspended to a cell density of 1×10^6 cells mL^{-1} and then loaded into the cell printer where it is printed into the micro-channels. The printing process is very short, typically 15–30 s per chip. Each print job uses 1 mL of cell suspension. This prints up to 20 layers with a total print time of at least 5 min. With a short print time and an actively moving cell suspension, the cells in the nozzle does not have sufficient amount of time to settle. In terms of cell aggregation, cells do gather together. Prior to printing, cells are pipetted to minimize aggregation. Once the cells are loaded into the microchannels, cell moves around and aggregate together during their initial attachment phase. The images taken (see the results and discussions section for images) during the biological investigation does not see the aggregation as an issue as the cells in the channels appears to be uniformly distributed.

3. Results and discussion

3.1. Cytotoxicity analysis

The first step in ensuring that this interconnected microfluidic chip is a potential pharmaceutical platform to characterize drugs is to investigate its biological relevance. There are several biological studies that are presented in this paper that illustrate strong evidence that this device is a good sensor for drug investigations. As discussed earlier, there are three pore sizes that are characterized; 300, 500, and 700 μm. Since the architecture is fabricated from photo-material that is enhanced for biocompatibility, it is important to characterize the cytotoxicity of the chip. The interactions of the cells within the micro-channels are of interest. Healthy cells have the ability to attach to the substrate and proliferate; this is an indicator that the substrate which the cells are growing on is not toxic. Biological assays such as fluorometric indicators and enzyme-linked immunosorbent assay are utilized to characterize the cytotoxicity of the chips.

Cytotoxicity analysis was conducted using a live/dead stain where live cells are stained green and dead cells are stained red. Calcein-AM (Dojindo, Japan, 1 μmol L^{-1}) is retained within the live cells, producing a green fluorescence while cells with damaged membranes allow the entrance of Propidium Iodide(Sigma-Aldrich, USA, 2 μmol L^{-1}) which undergoes a fluorescence enhancement upon binding to nucleic acids promoting a red fluorescence in dead cells. Prior to characterization, chips were washed three times with PBS then stained with both reagents and incubated at 37 °C for 15 min. After incubation, chips were washed three times with PBS to remove the reagents. The washed chips were then observed under a laser scanning confocal microscope(Zeiss 710 META, Germany).

The 300, 500, and 700 μm chips showed similar fluorescence results in terms of cells growing within the channels of the chips. Figures 5(*A*2), (*B*2), (*C*2) shows a set of fluorescence images of live cells stained green using the live:dead assay. These images highlight the live cell's orientation and uniformity within the channels of each chip. *A*1 is a fluorescence image of a channel in the 300 μm pore

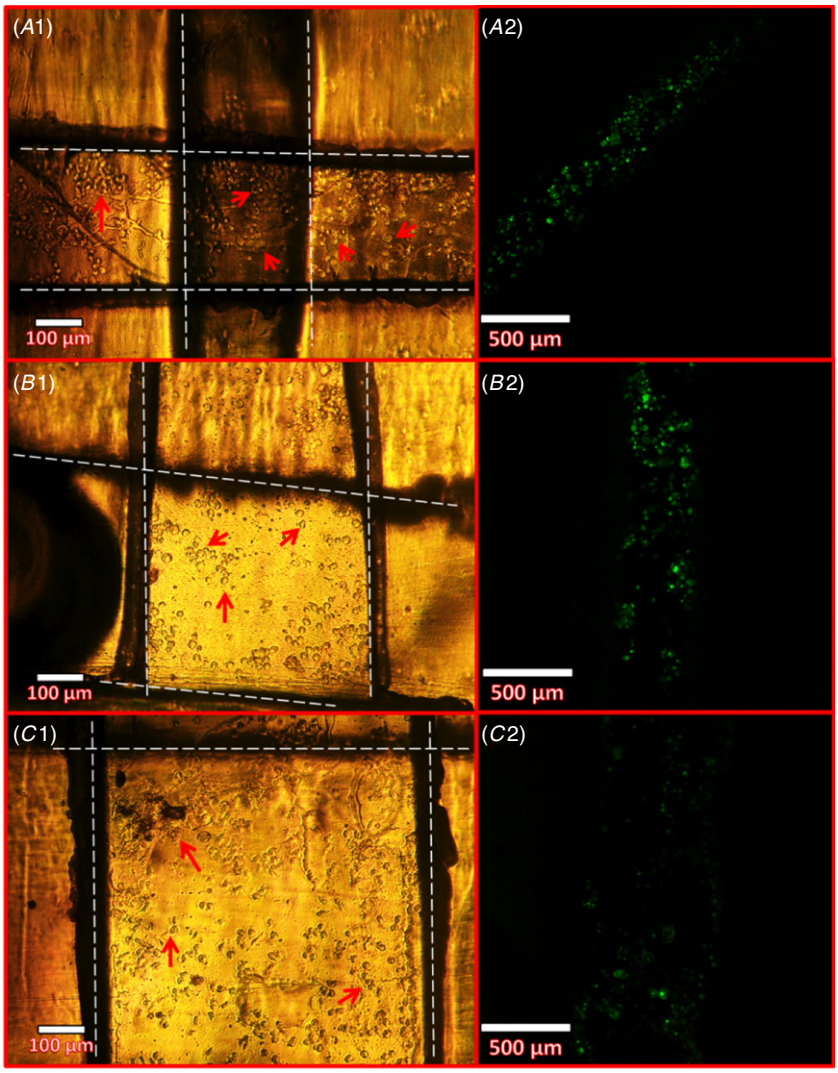

Figure 5. (*A*1), (*B*1), (*C*1) Optical images of a pore of the interconnected chips. The dashed lines highlights the channel walls, the arrow points at cells within the channels. *A*1 is an optical image of a 300 μm pore chip, *B*1 is an optical image of a 500 μm pore chip, and *C*1 is an optical image of a 700 μm pore chip. (*A*2), (*B*2), (*C*2) are fluorescence images of the live cells stained green with the live dead assay. These images highlight the live cell's orientation and uniformity within the channels of each chip. *A*1 is a fluorescence image of a channel in the 300 μm pore chip, *B*2 is a fluorescence image of a channel in the 500 μm pore chip, and *C*2 is a fluorescence image of a channel in the 700 μm pore chip.

chip, *B*2 is a fluorescence image of a channel in the 500 μm pore chip, and *C*2 is a fluorescence image of a channel in the 700 μm pore chip. As seen these images, there are a significant amount of live cells (stained green) growing within the chips, this trend was observed with all chips and is confirmed by the proliferation study (figure 6). During this investigation, not much red fluorescence (dead cells) was observed. This is due in part that when cells die they detaches from the surface on which they were attached to while they were alive and actively proliferating. Additionally, when these cells die, they tend to float in the culture medium. During the confocal preparation, samples were washed three times and at this stage any/all dead cells within the channels were washed away.

Figures 5(*A*1), (*B*1), (*C*1) are optical images of a pore of the interconnected chips. The dashed lines highlights the channel walls, the arrow points at cells within the channels. *A*1 is an optical image of a 300 μm pore chip, *B*1 is an optical image of a 500 μm pore chip, and *C*1 is an optical image of a 700 μm pore chip. Due to the chip's design and characterization limitations, it is difficult to capture a full three-dimensional view of the cells within the channels. SEM characterization can be used to give an in-depth view of the cells within the channels. However, since the cells are deep inside the enclosure, it would require sectioning the chip to view the inside. Doing this would destroy the sample. Optical imaging does not interfere with the sample and presents and idea of what is happening inside the chip. These optical images present an overview of the differences within the pores, overlay of the two layers, and the distribution of cell within the channel. Due to equipment limitations, only one channel can be viewed at once. What is presented in the optical images, in terms of cell distribution, is true for both layers throughout the chip's architecture.

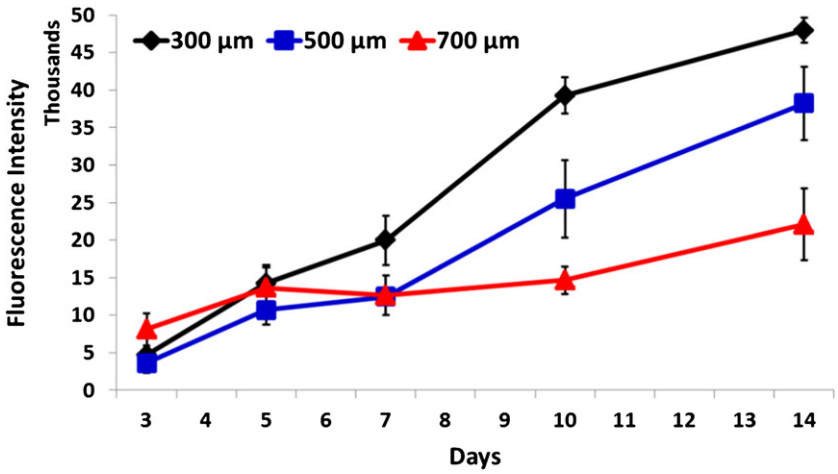

Figure 6. Results of the 14 day proliferation investigation of the 300, 500, and 700 μm micro-fluidic chips.

3.2. Cell interactions

Cell interactions within the channels play an important role in the development of a fully functional pharmaceutical sensor [52]. A fluorometric investigation was conducted which characterized the cell–cell interaction and proliferation within the fabricated chips. This characterization was performed with the use of AbD SeroTEC's Alamar Blue (Ab). The cell-laden chips were washed with 1x phosphate buffered saline (PBS) by pumping the PBS through the chips with a syringe pump at a flow rate of 30 μL h^{-1} 10% Ab was mixed with culture medium and was pumped through the chips at 30 μL h^{-1} until the chips were filled with the reagent. The chips were then disconnected from the syringe pump and were placed in the incubator for 4 h. After 4 h, the resulting reagent within the chips were removed from the chips and characterized with a microplate reader (GENios, TECAN, North Carolina, USA) whose excitation and emission wavelengths were 535 nm and 590 nm respectively. The results from this study are shown in figure 6.

All chips in the proliferation study showed an increasing trend of cell proliferation. According to the data, the chips with the 300 μm pore size had the highest number of cells within the 14 day study, followed by the 500 μm pore size and the 700 μm pore size chips, respectively. The high surface area to volume ratio and shear stress within the pores/channels may be credited for the higher number of cells within the smaller pore sized chip [53]. Additionally, at the beginning of the 14 day study, the 700 μm pore chip had the higher number of cells in its chip. Since the 700 μm chip had the widest channels, a higher volume of cell-suspension was required to fill the channel during the 'cell printing' process. At the end of the study, the 700 μm chip had the lowest cell count and there is a slow progression of growth throughout the investigation. A lower shear stress and limited cell-to-cell interaction due to wide channels are two factors that may have contributed to the slowed growth of the 700 μm channel. The 300 μm and the 500 μm chips have similar proliferation trends with the only difference being a lower cell count in the 500 μm chip at the beginning of the study; this may have contributed to the 500 μm chip having a lower cell number at the end of the study in comparison to the 300 μm chip.

3.3. Drug metabolism

To demonstrate effective drug metabolism within the three interconnect chips, a drug is fed into the chip through the inlet port and metabolized by the cells. Results of this analysis are used to understand the relative pharmacokinetic efficiency and relevancy interconnected microfluidics. The drug flow study protocol includes 120 μL of 10 mM EFC (7-ethoxy-4-trifluoromethyl coumarin) (Sigma-Aldrich) stock solution mixed with 9.88 ml of MDA MB 231 complete cell culture medium. The working solution is perfused into a syringe and infused into the chips with the syringe pump at a flow rate of 30 μL h^{-1} until the chip is completely filled. Chips are then incubated with static, non-perfused controls until characterization. During the incubation period, the drug substrate is metabolized by the cells into the metabolite. This metabolism process converts the drug 7-ethoxy-4-(trifluoromethyl)coumarin (EFC) to 7-hydroxy-4-(trifluoromethyl)coumarin (HFC) by the enzyme 7-ethoxycoumarin O-deethylase [45, 54]. Due to characterization limitations, the cells within the chip cannot be characterized, hence the effluent is characterized to demonstrate effective drug metabolism. On hours 3, 6, 9, and 12 the effluent is extracted from the chips and is quantified with a microplate reader (TECAN, GENios). The EFC measured directly correlates to the HFC within the cell. As the measured EFC decreases, the HFC increases.

After 12 h there is a trace of the EFC drug concentration found in the 500 and 700 μm chips and none in the 300 μm chips. The 300 μm chip demonstrated the sharpest decline of the EFC drug concentration in the effluent followed by the 500 and 700 μm chips, respectively. At 6 h, the 700 μm chip had the least amount of EFC drug concentration. This may be due to the large pores within the chip that allows great diffusion of the drug within the chip. Since equal amounts of cells were seeded into the chips, the difference of EFC drug concentrations are due to the pores within the chips. Overall, after 12 h; cells in the 300 μm chip absorbed the EFC drug

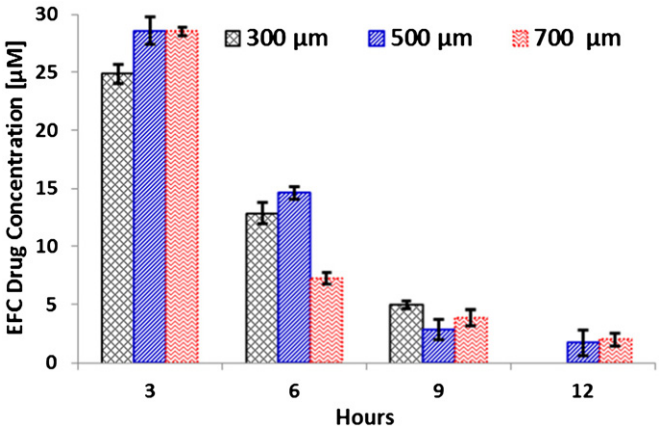

Figure 7. Results of the EFC drug concentration in the 300, 500, and 700 μm chips over a 12 h period.

faster compared to the 500 and 700 μm. With the exception at the 6 h mark, cells in the 500 and 700 μm chips seem to absorb the EFC drug at the same rate. Figure 7 shows the results of the drug metabolism study.

3.4. Cell morphology and structural integrity

Cell morphology and the internal micro-architecture were evaluated using an FEI/Philips XL-30 field emission environmental scanning electron microscope (SEM). The images obtained from the SEM were taken using a beam intensity of 2 kV and gaseous secondary electron detectors of 1.3 Torr. Prior to SEM investigation of the micro-architecture, the appropriate preparation was conducted by first sectioning the chip using a sharp straight razor. Since the ion beam cannot penetrate the PDMS layer, sectioning the chip is the only way the view the internal features. The method of sectioning does cause some deformation to the internal features by causing the layers to separate a little. Although the internal features a slightly displaced, the SEM image shown in figure 8(*A*) illustrates the internal architecture, interconnectivity, channel formation, porosity, and structural integrity of the fabricated chips. SEM was conducted on all chips and each chip shown similar structural integrity (illustrated in figure 8(*A*)).

Figure 8(*B*) is an SEM image taken to illustrate the morphology of the cells within the chips. The SEM preparation for these samples required the chips to be washed twice with 1x PBS (pumped through the chips). Then the cells were fixed with 4% glutaraldehyde (Sigma Aldrich, USA) for 2 h. After being fixed, each chip was subjected to dehydration by pumping a series of diluted ethanol (50%, 70%, 90%, 95%, and 100%) through each chip. After the dehydration process, chips were dried and refrigerated at 4 °C for 24 h. Prior to SEM characterization, each chip was sectioned to remove the PDMS layer. As seen in the SEM image, the cells are well anchored within the chip and showed signs of active proliferation. The morphology differs in comparison to two-dimensional tissue culture, but is consistent to that of a three-dimensional tissue culture.

3.5. Computational analysis

The microfluidic chips presented are not conventional single flow chips. These chips have interconnected channels and are elevated to 1 mm in total height. The fluids within the chips are actuated with the use of an external actuator (programmable syringe pump). Microfluidics with an external actuator is classified as continuous-flow microfluidics. Due to the complex architectural design and fluid flow of each chip, a computational analysis is needed to illustrate the velocity gradient and fluid flow.

COMSOL Multiphysics® was used to characterize the fluid flow within the 300, 500, and 700 μm microfluidic chips. COMSOL's microfluidic module is widely used to study microfluidic devices. The flow of a fluid through a microfluidic channel can be characterized by Reynolds number using equation (1):

$$\mathrm{R_e} = \frac{LV_{\mathrm{avg}}\rho}{\mu} \tag{1}$$

where L is the length scale which equals to four times the cross-sectional area over the wetted perimeter of the channel (4A/P), μ is the viscosity, ρ is the fluid density, and V_{avg} is the average velocity of the flow. $\mathrm{R_e}$ is often less than 1.0 due to the small dimensions of microchannels. In this Reynolds number regime, flow is completely laminar and no turbulence occurs.

The boundary conditions for the inlet of each chip are set at the flow rate of the syringe pump, 30 μL h^{-1}, while the outlet pressure was set at 0 Pa. The cell culture medium was simulated through the chips with a density of 1×10^3 kg m^{-3} and a dynamic viscosity of 1×10^{-3} Pas for a period of one hour. COMSOL's microfluidic module solves the Navier–Stokes equations:

$$\rho\frac{\partial u}{\partial t} - \nabla \cdot \mu(\nabla u + (\nabla u)^T) + \rho u \cdot \nabla u + \nabla p = 0 \tag{2}$$

where ρ denotes density (kg m^{-3}), u is the velocity (m/s), μ denotes dynamic viscosity (Pas), and p equals pressure (Pa).

Figure 9 illustrates the simulation results showing the fluid velocity gradient and the streamline within the 300, 500, and 700 μm microfluidic chips. The streamline plots are featured to illustrate the fluid flow throughout the interconnective pores. In each streamline plot, starting point control was applied with 100 lines originating from the inlet. On the other hand the velocity gradient plots illustrate fluid direction, magnitude, and most importantly, flow type. Each microfluidic chip is utilized for their ability to produce laminar flow within its channels. However, when the architecture is complex, a simulation is beneficial to capture the flow type within the chip. A set of parallel velocity vector indicates laminar flow, else it is turbulent. The simulation results are conclusive and states that laminar flow exist in the 300, 500, and 700 μm microfluidic chips. Additionally, the streamline plot for the 300, 500, and 700 μm microfluidic chips demonstrate that the fluid is interconnective. These claims are proven correct in figure 9 where (*A*1) is a streamline simulation of the fluid flow within the 300 μm interconnected channels. (*A*2) is a velocity gradient showing the magnitude, direction, and fluid flow type that exist throughout the 300 μm microfluidic chip. (*A*3) is a close-up of the velocity gradient at one of the interconnected pore within

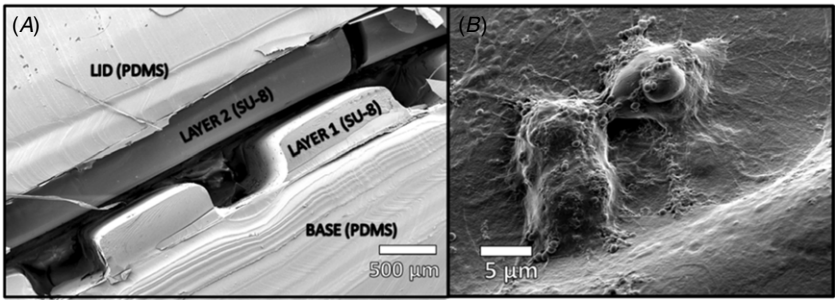

Figure 8. (*A*) A SEM images showing the cross-sectional of a micro-fluidic chip. This image illustrates the channel's formation and structural integrity. Each chip showcases the same formation and structural integrity with their corresponding varying channel width. (*B*) A SEM image showing the morphology and attachment of the MDA-MB-231 cells within the micro-channel of the chip.

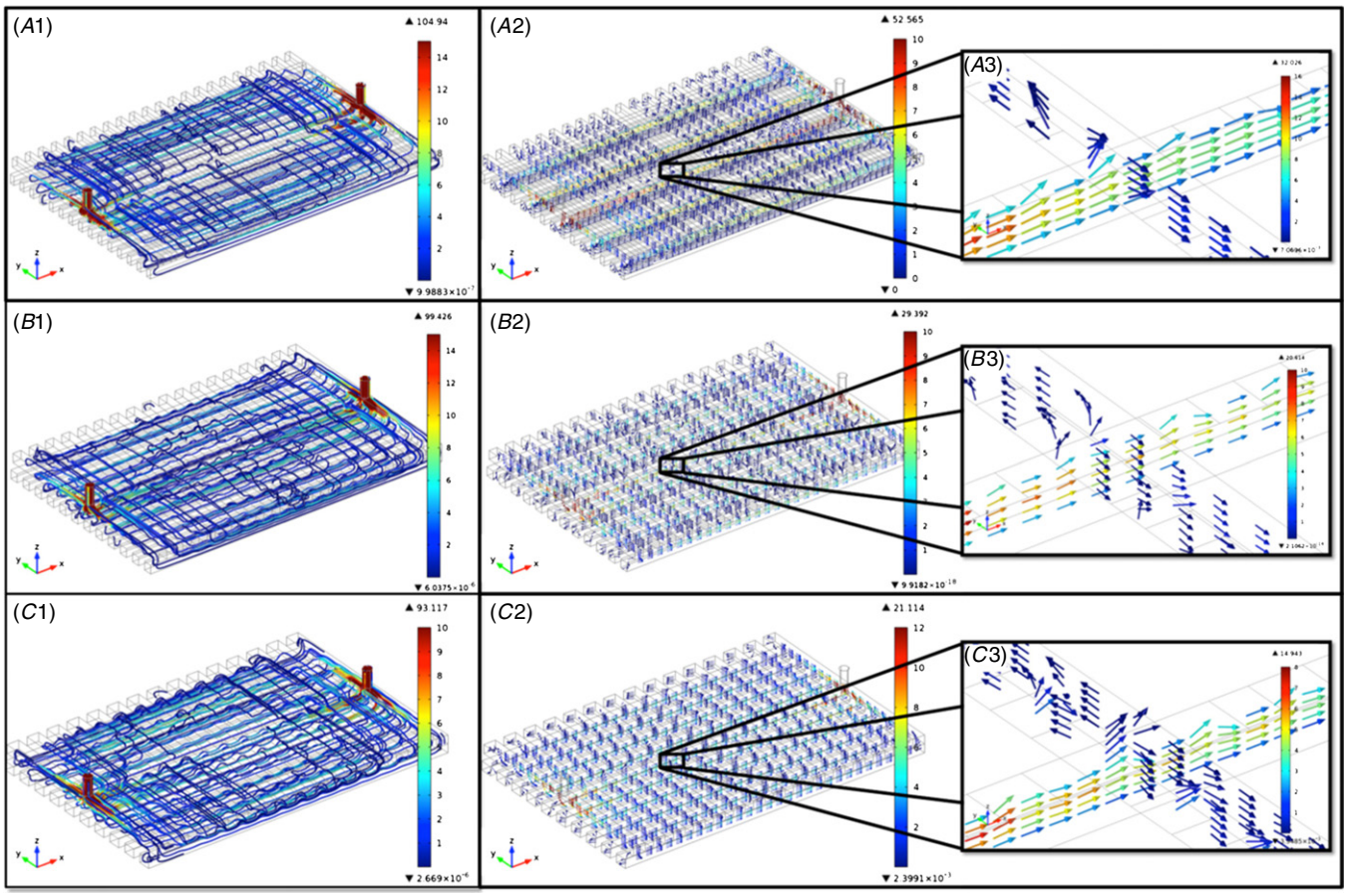

Figure 9. COMSOL multiphysics simulations illustrating the fluid flow within the 300, 500, and 700 μm microfluidic chips. (*A*1) is a streamline simulation of the fluid flow within the 300 μm interconnected channels. (*A*2) is a velocity gradient showing the magnitude, direction, and fluid flow type that exist throughout the 300 μm microfluidic chip. (*A*3) is a close-up of the velocity gradient at one of the interconnected pore within the 300 m microfluidic chip. (*B*1) is a streamline simulation of the fluid flow within the 500 μm interconnected channels. (*B*2) is a velocity gradient showing the magnitude, direction, and fluid flow type that exist throughout the 500 μm microfluidic chip. (*B*3) is a close-up of the velocity gradient at one of the interconnected pore within the 500 μm microfluidic chip. (*C*1) is a streamline simulation of the fluid flow within the 700 μm interconnected channels. (*C*2) is a velocity gradient showing the magnitude, direction, and fluid flow type that exist throughout the 700 μm microfluidic chip. (*C*3) is a close-up of the velocity gradient at one of the interconnected pore within the 700 μm microfluidic chip. Color scale bar unit: μm s^{-1}

the 300 m microfluidic chip. (*B*1) is a streamline simulation of the fluid flow within the 500 μm interconnected channels. (*B*2) is a velocity gradient showing the magnitude, direction, and fluid flow type that exist throughout the 500 μm microfluidic chip. (*B*3) is a close-up of the velocity gradient at one of the interconnected pore within the 500 μm microfluidic chip. (*C*1) is a streamline simulation of the fluid flow within the 700 μm interconnected channels. (*C*2) is a velocity gradient showing the magnitude, direction, and fluid flow type that exist throughout the 700 μm microfluidic chip. (*C*3) is a close-up of the velocity gradient at one of the interconnected pore within the 700 μm microfluidic chip.

3.6. Limitations

The digital micro-mirroring device is a fast and an economic approach of fabricating micro-arrays. One of its greatest limitations is the size of its structures that can be produced. The mirrors itself is no bigger than 0.7 inches (17.78 mm) in length. With the use of optics the projected pattern can fabricate larger structures; however, it comes with a loss of resolution. Additional layers are fabricated by aligning an optical mask onto a physical pattern. As the layer increases it becomes increasingly difficult to accurately align additional layer. This system has limitations when it comes to fabricating large micro-structures. Besides size limitations, this device is also limited to only photo-sensitive materials. The DBD plasma system is idea for localize plasma treatment. As the treatment area increases, the total treatment time will increase. For large structure it will take an increasingly long time to complete the treatment process. The biologics deposition system is similar to the DBD plasma, as they both focuses on developing micro-arrays.

The three-dimensional cell-laden microfluidic chip is a unique product that is developed to culture cells in a micro-fluidic environment with directly perfusion with the capability to investigate drug metabolism. Many three-dimensional tissue scaffolds fabricated culture their cells in a static environment which often lead to a lack of nutrients getting to the center of the scaffold. Additionally, tissue scaffold tends to be large and slightly bulky. The architecture of this microfluidic chip is small, interconnected (same as tissue scaffolds), and most importantly, there is a laminar flow perfusion of culture medium throughout the chip. The small design allows for only a few thousand of cells to complete seed the array, this is an economical benefit. This system is advantageous; however, it is not flawless. Due to its design these chips can only be used once. Once the chips are sealed they have to be sectioned to gain access to the inside. The only way to get materials such as cultures and assay to the cells is to pump it through it inlet. Additionally, due to its small size, any characterizations conducted will result in small volumes. This cell-laden microfluidic chip is ideal for investigations where the samples (fluid characterized) are small and of course, since drugs are expensive; it allows for economic drug studies. The development of each micro-fluidic system is specifically designed for a targeted objective. There are several three-dimensional micro-fluidic systems that currently exist, each with its own unique functionality [42, 55, 56].

4. Conclusions

This paper presents an integrative fabrication technique to develop three-dimensional interconnected microfluidic tissue arrays for pharmaceutical investigations using digital microfabrication, biologics printing, and plasma treatment. The architecture of the sensor is fabricated using digital photolithographic method while the biologics are embedded within the channels of the internal architecture of chip. Additionally, this paper illustrates the need for plasma treatment of the photo-material used to develop the micro-architecture of this chip. This sensor is proven to be a successful tissue array for pharmaceutical investigation by several characterization methods. Biological characterizations were performed on each chipset to demonstrate its potential to host live cells in an interconnected microfluidic chip. The biological results from the three chipset demonstrated that within the 14 days, cells attached and proliferated within the interconnected microfluidic environment. Of the three chips studied, the 300 μm chip had the best cell proliferation, followed by the 500 μm and the 700 μm chip. Additionally, the drug up-take was slightly better in the 300 μm chips compared to the 500 μm and the 700 μm chips. SEM characterization were performed to study the cell morphology within the channels, as it is known that cells in a three-dimensional environment have a different morphology in comparison to that of two-dimensional cultures; this was proven true with the SEM investigation. Structural integrity is another focus of this paper. It is understood that within the micro-features of this sensor, it would be possible to develop a platform for pharmaceutical investigations. The SEM confirms that all chips fabricated are interconnected where the channels are uniformity distributed within their respective layers. The fabrication procedures and characterizations illustrated in this paper demonstrate that the sensor developed in this paper is a good addition for drug investigations.

Acknowledgments

National Science Foundation grant no 1209517 and NSF-CMMI-1030520 are acknowledged for the support of this project.

References

[1] Shor L 2008 Novel fabrication development for the application of polycaprolactone and composite polycaprolactone/ hydroxyapotote scaffolds for bone tissue engineering *PhD Dissertation*, Drexel University, Philadelphia, PA
[2] Starly B 2006 Biomimetic design and fabrication of tissue engineered scaffolds using computer aided tissue engineering *PhD Dissertation* Drexel University, Philadelphia, PA
[3] Judy J W 2001 Microelectromechanical systems (MEMS): fabrication, design and applications *Smart Mater. Struct.* **10** 1115–34
[4] Senturia S D, Harris R M, Johnson B P, Kim S, Nabors K, Shulman M A and White J K 1992 A computer-aided design system for microelectromechanical systems (MEMCAD) *J. Microelectromech. Syst.* **1** 3–13
[5] Bao M and Wang W 1996 Future of microelectromechanical systems (MEMS) *Sensors Actuators* A **56** 135–41
[6] Jo B H, Van Lerberghe L M, Motsegood K M and Beebe D J 2000 Three-dimensional micro-channel fabrication in polydimethylsiloxane (PDMS) elastomer *J. Microelectromech. Syst.* **9** 76–81
[7] Despa M S, Kelly K W and Collier J R 1999 Injection molding of polymeric LIGA HARMs *Microsyst. Technol.* **6** 60–66
[8] Heckele M and Schomburg W K 2004 Review on micro molding of thermoplastic polymers *J. Micromech. Microeng.* **14** R1–4
[9] Cho Y-R, Oh J-Y, Kim H-S and Jeong H-S 1999 Micro-etching technology of high aspect ratio frameworks for electronic devices *Mater. Sci. Eng.* B **64** 79–83

[10] Hawkeye M M and Brett M J 2007 Glancing angle deposition: fabrication, properties, and applications of micro- and nanostructured thin films *J. Vac. Sci. Technol.* A **25** 1317–35

[11] Staples M, Daniel K, Cima M and Langer R 2006 Application of micro- and nano-electromechanical devices to drug delivery *Pharm. Res.* **23** 847–63

[12] Arora A, Prausnitz M R and Mitragotri S 2008 Micro-scale devices for transdermal drug delivery *Int. J. Pharm.* **364** 227–36

[13] Beebe D J, Mensing G A and Walker G M 2002 Physics and applications of microfluidics in biology *Annu. Rev. Biomed. Eng.* **4** 261–86

[14] Sia S K and Whitesides G M 2003 Microfluidic devices fabricated in poly(dimethylsiloxane) for biological studies *Electrophoresis* **24** 3563–76

[15] Sun C, Fang N, Wu D M and Zhang X 2005 Projection micro-stereolithography using digital micro-mirror dynamic mask *Sensors Actuators* A **121** 113–20

[16] Lu Y, Mapili G, Suhali G, Chen S and Roy K 2006 A digital micro-mirror device-based system for the microfabrication of complex, spatially patterned tissue engineering scaffolds *J. Biomed. Mater. Res.* A **77A** 396–405

[17] Singh-Gasson S, Green R D, Yue Y, Nelson C, Blattner F, Sussman M R and Cerrina F 1999 Maskless fabrication of light-directed oligonucleotide microarrays using a digital micromirror array *Nature Biotechnol.* **17** 974–8

[18] Chen L, McBranch D W, Wang H L, Helgeson R, Wudl F and Whitten D G 1999 Highly sensitive biological and chemical sensors based on reversible fluorescence quenching in a conjugated polymer *Proc. Natl Acad. Sci. USA* **96** 12287–92

[19] Janata J and Josowicz M 2003 Conducting polymers in electronic chemical sensors *Nature Mater.* **2** 19–24

[20] Janata J 2009 *Principles of Chemical Sensors* (Berlin: Springer)

[21] Lowe C 1985 An introduction to the concepts and technology of biosensors *Biosensors* **1** 3–16

[22] Davis G 1985 Electrochemical techniques for the development of amperometric biosensors *Biosensors* **1** 161–78

[23] Lavrik N V, Sepaniak M J and Datskos P G 2004 Cantilever transducers as a platform for chemical and biological sensors *Rev. Sci. Instrum.* **75** 2229–53

[24] Tibbitt M W and Anseth K S 2009 Hydrogels as extracellular matrix mimics for 3D cell culture *Biotechnol. Bioeng.* **103** 655–63

[25] Arnold M and Rechnitz G 1981 Selectivity enhancement of a tissue-based adenosine-sensing membrane electrode *Anal. Chem.* **53** 515–8

[26] Liu Y, Dong X and Chen P 2012 Biological and chemical sensors based on graphene materials *Chem. Soc. Rev.* **41** 2283–307

[27] Mironov V, Trusk T, Kasyanov V, Little S, Swaja R and Markwald R 2009 Biofabrication: a 21st century manufacturing paradigm *Biofabrication* **1** 022001

[28] Rudolph A S and Reasor J 2001 Cell and tissue based technologies for environmental detection and medical diagnostics *Biosens. Bioelectron.* **16** 429–31

[29] Wilson W C and Boland T 2003 Cell and organ printing: I. Protein and cell printers *Anat. Rec. A: Discov. in Mol. Cell. Evol. Biol.* **272** 491–6

[30] Mironov V, Boland T, Trusk T, Forgacs G and Markwald R R 2003 Organ printing: computer-aided jet-based 3D tissue engineering *Trends Biotechnol.* **21** 157–61

[31] Sun W, Darling A, Starly B and Nam J 2004 Computer-aided tissue engineering: overview, scope and challenges *Biotechnol. Appl. Biochem.* **39** 29–47

[32] Chang R, Nam J and Sun W 2008 Direct cell writing of 3D microorgan for *in vitro* pharmacokinetic model *Tissue Eng.* **14** 157–66

[33] Khalil S, Nam J and Sun W 2005 Multi-nozzle deposition for construction of 3D biopolymer tissue scaffolds *Rapid Prototyping J.* **11** 9–17

[34] Bidan G 1992 Electroconducting conjugated polymers: new sensitive matrices to build up chemical or electrochemical sensors. A review *Sensors Actuators* B **6** 45–56

[35] Azad A, Akbar S, Mhaisalkar S, Birkefeld L and Goto K 1992 Solid-state gas sensors: a review *J. Electrochem. Soc.* **139** 3690–704

[36] Aernecke M, Snow E, Knight L B, Malliaras G G and Tok J B H 2008 *Nano and Microsensors for Chemical and Biological Terrorism Surveillance* (Cambridge: RSC Books)

[37] Sparks D, Smith R, Straayer M, Cripe J, Schneider R, Chimbayo A, Anasari S and Najafi N 2003 Measurement of density and chemical concentration using a microfluidic chip *Lab Chip* **3** 19–21

[38] Thorsen T, Roberts R W, Arnold F H and Quake S R 2001 Dynamic pattern formation in a vesicle-generating microfluidic device *Phys. Rev. Lett.* **86** 4163–6

[39] Thompson C A, Colon-Hernandez P, Pomerantseva I, MacNeil B D, Nasseri B, Vacanti J P and Oesterle S N 2002 A novel pulsatile, laminar flow bioreactor for the development of tissue-engineered vascular structures *Tissue Eng.* **8** 1083–8

[40] Yildirim E D, Ayan H, Vasilets V N, Fridman A, Guceri S and Sun W 2008 Effect of dielectric barrier discharge plasma on the attachment and proliferation of osteoblasts cultured over poly (ε-caprolactone) scaffolds *Plasma Process. Polym.* **5** 58–66

[41] Yildirim E D, Besunder R, Pappas D, Allen F, Güçeri S and Sun W 2010 Accelerated differentiation of osteoblast cells on polycaprolactone scaffolds driven by a combined effect of protein coating and plasma modification *Biofabrication* **2** 014109

[42] Han Y L, Wang W, Hu J, Huang G, Wang S, Lee W G, Lu T and Xu F 2013 Benchtop fabrication of three-dimensional reconfigurable microfluidic devices from paper/polymer composite *Lab Chip* **13** 4745–9

[43] Laimer J and Störi H 2007 Recent advances in the research on non-equilibrium atmospheric pressure plasma jets *Plasma Processes and Polymers* vol 4 (Weinheim: Wiley) pp 266–74

[44] Eckstein F *et al* 2008 Precision of 3.0 tesla quantitative magnetic resonance imaging of cartilage morphology in a multicentre clinical trial *Ann. Rheum. Dis.* **67** 1683–8

[45] Chang R and Sun W 2009 Biofabrication of three-dimensional liver cell-embedded tissue constructs for *in vitro* drug metabolism models (Saarbrücken: OmniScriptum)

[46] Sun W, Darling A, Starly B and Nam J 2004 Computer-aided tissue engineering: overview, scope and challenges *Biotechnol. Appl. Biochem.* **39** 29–47

[47] Sun W and Lal P 2002 Recent development on computer aided tissue engineering—a review *Comput. Methods Programs Biomed.* **67** 85–103

[48] Nederman T, Acker H and Carlsson J 1983 Penetration of substances into tumor tissue: a methodological study with microelectrodes and cellular spheroids *In Vitro* **19** 479–88

[49] Sant S, Tao S L, Fisher O, Xu Q, Peppas N A and Khademhosseini A 2011 Microfabrication technologies for oral drug delivery *Adv. Drug Deliv. Rev.* **64** 496–507

[50] Karageorgiou V and Kaplan D 2005 Porosity of 3D biomaterial scaffolds and osteogenesis *Biomaterials* **26** 5474–91

[51] O'Brien F J, Harley B, Yannas I V and Gibson L J 2005 The effect of pore size on cell adhesion in collagen-GAG scaffolds *Biomaterials* **26** 433–41

[52] Koh H, Yong T, Chan C and Ramakrishna S 2008 Enhancement of neurite outgrowth using nano-structured scaffolds coupled with laminin *Biomaterials* **29** 3574

[53] Karande T S, Ong J L and Agrawal C M 2004 Diffusion in musculoskeletal tissue engineering scaffolds: design issues related to porosity, permeability, architecture, and nutrient mixing *Ann. Biomed. Eng.* **32** 1728–43

[54] Donato M T, Jiménez N, Castell J V and Gómez-Lechón M J 2004 Fluorescence-based assays for screening nine cytochrome P450 (P450) activities in intact cells expressing individual human P450 enzymes *Drug Metab. Dispos.* **32** 699–706

[55] Chiu D T, Jeon N L, Huang S, Kane R S, Wargo C J, Choi I S, Ingber D E and Whitesides G M 2000 Patterned deposition of cells and proteins onto surfaces by using three-dimensional microfluidic systems *Proc. Natl Acad. Sci. USA* **97** 2408–13

[56] Bettinger C J, Weinberg E J, Kulig K M, Vacanti J P, Wang Y, Borenstein J T and Langer R 2005 Three-dimensional microfluidic tissue-engineering scaffolds using a flexible biodegradable polymer *Adv. Mater.* **18** 165–9